Fluorescence correlation spectroscopy on electron transfer reactions : probing inter- and intramolecular redox processes

Sen, S.

Citation

Sen, S. (2016, June 30). *Fluorescence correlation spectroscopy on electron transfer reactions : probing inter- and intramolecular redox processes*. *Casimir PhD Series*. Retrieved from https://hdl.handle.net/1887/40761

Version:	Not Applicable (or Unknown)
License:	[Licence agreement concerning inclusion of doctoral thesis in the Institutional Repository of the University of Leiden](#)
Downloaded from:	https://hdl.handle.net/1887/40761

Note: To cite this publication please use the final published version (if applicable).

Cover Page

Universiteit Leiden

The handle http://hdl.handle.net/1887/40761 holds various files of this Leiden University dissertation.

Author: Sen, S.
Title: Fluorescence correlation spectroscopy on electron transfer reactions : probing inter- and intramolecular redox processes
Issue Date: 2016-06-30

Chapter 1

Introduction

This chapter is a general introduction to the work presented in this thesis. A brief overview of the protein investigated, as well as the techniques used is presented. At the end, a short synopsis of each of the following chapters is provided.

1.1 *Introduction*

Redox reactions are the foundation of life. They encompass a variety of oxidation and reduction processes such as photosynthesis, redox homeostasis, cellular respiration, water oxidation and metabolism. Most importantly, enzymes are needed to make those redox reactions effective and to control them. Some of the most demanding reactions such as nitrogen fixation and photosynthesis are driven by redox active metalloproteins, enzymes that generally use small, inorganic or organic cofactors to execute those reactions. Metals such as vanadium, manganese, iron, cobalt, nickel, copper, zinc, magnesium and calcium have been found to play essential roles in the structure and function of metalloproteins(*1*)(*2*) (See Fig.1.1 for a few examples). In this thesis, the spotlight is on a redox active bacterial copper protein, azurin, which is mostly involved in the shuttling of electrons, i.e., electron transfer (ET) processes with other proteins or molecules in the cell. This feature of the protein has been exploited in many studies of protein-protein interactions, ET processes or catalysis. They have opened up new possibilities for applications in biotechnology and biosensors.

One way of monitoring ET or redox reactions is by electrochemistry such as cyclic voltammetry and protein film voltammetry. These techniques often require the surface confinement of an enzyme on an appropriately modified electrode. Since the redox cofactors or the prosthetic groups usually lay deeply buried inside the protein matrix(*3*)(*4*) and since there is limited control of the protein orientation, this may cause pathway uncertainties and heterogeneity of the ET rates.
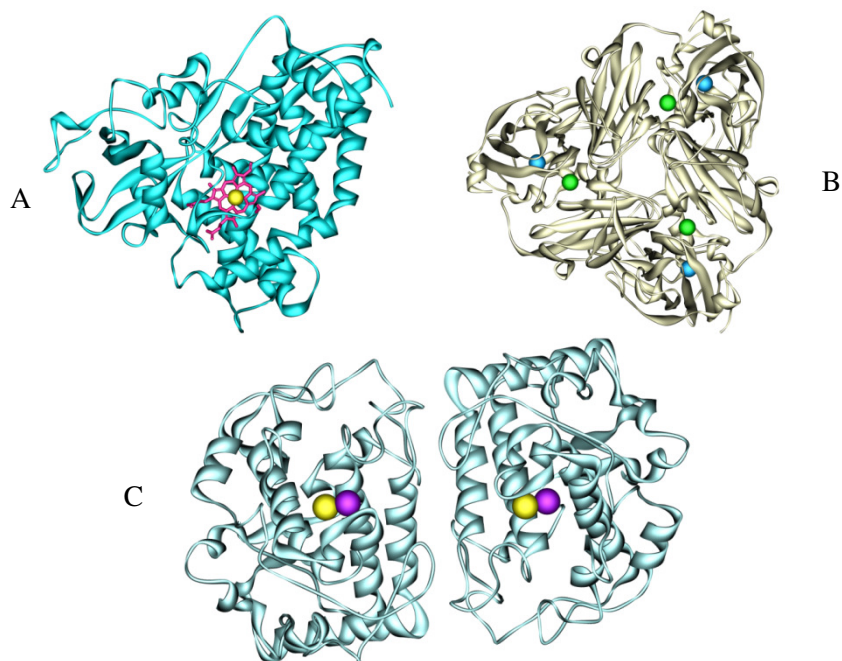
Figure 1.1: *Crystal structures of metalloproteins. (A) 1DZ4*: Cytochrome P450cam from Pseudomonas putida, a heme mono-oxygenase that catalyses the reaction of hydrocarbons with molecular oxygen at ambient temperature; the porphyrin group is shown in pink stick, and the iron ion is shown as a yellow sphere, (B) 2PP9*: Nitrite reductase from Alcaligenes faecalis S-6, a copper-containing protein that catalyses the production of nitric oxide from nitrite; the green spheres show the Type II copper centers and the blue spheres represent the Type I centers in the active sites, (C) 4P6R*: Tyrosinase from Bacillus megaterium, responsible for the conversion of tyrosine to melanine; copper centers are shown as yellow and violet spheres.*

*: The codes refer to the PDB accession numbers in the protein data bank (www.rcsb.org and H.M. Berman, J. Westbrook, Z. Feng, G. Gilliland, T.N. Bhat, H. Weissig, I.N. Shindyalov, P.E. Bourne (2000) The Protein Data Bank, Nucleic Acids Research, 28: 235-242.)

Singlemolecule techniques have provided direct access to the behavior of an individual molecule in solution. Single-molecule studies often make use of fluorescence imaging techniques. With this approach, the behavior of a single protein molecule, or of short-lived intermediates in a reaction can be monitored in time(*5*)(*6*)(*7*)(*8*)(*9*)(*10*). Reaction mechanisms can be investigated in detail, and the possible individual variations in a population of molecules can be accessed. The objective of the research described in this thesis is to obtain information on the heterogeneity of the activity of a redox protein via a single-molecule approach.

1.2 *Copper proteins*

Copper is an essential element for living organisms. It occurs in a variety of metalloproteins, many of which are involved in oxygen binding, blood coagulation and electron transfer and redox reactions based on the Cu(I)/Cu(II) couple. Examples are plastocyanin, rusticyanin, laccase, terminal oxidase, oxygenase, superoxide dismutase, and ceruloplasmin. The properties and activities of these copper proteins are well documented(*11*)(*12*)(*13*)(*14*). Cu(I) is a soft acid while Cu(II) is a borderline case. Thus, the copper binding sites are ligated by side chains with soft or borderline ligands e.g. nitrogen donor atoms from histidine and sulfur atoms from cysteine/methionine. These ligands are preferred over hydroxyl and carboxyl groups or primary amine-side chains, as found in serine and tyrosine, aspartate and glutamate, and asparagine, glutamine, and arginine residues, respectively. Three main types of copper centers have been documented in the literature. (a) Type I copper proteins have a beautiful blue color, far more intense than the color of synthetic copper complexes in solution, but similar in hue. They are also called cupredoxins and have a strong absorption around 600 nm. In general, their Cu-coordination sphere is based on two histidines and one cysteine. The coordination sphere may be completed by a methionine or a leucine. Type I proteins are characterized by EPR spectra exhibiting small copper hyperfine couplings and small g-anisotropy; e.g. azurin, plastocyanin and nitrite reductase(*1*), (b) Type II Cu, occurring in "non-blue" copper proteins, has an essentially planar coordination sphere with 2-3 histidines and oxygen from a carboxylic group. A water molecule or hydroxide ion is often found as additional coordinating ligand. These proteins have a weak absorption in the visible region, and EPR spectra with axial symmetry; e.g. galactose oxidase, amine oxidase, dopamine mono oxidase carry a Type II active site(*15*), (c) Type III proteins contain a dinuclear copper center with a Cu-Cu distance of ~ 350 pm; after oxygen uptake, they show absorptions at 350 nm and 600 nm, e.g. haemocyanin and tyrosinase. These proteins are EPR silent as the copper centers are anti-ferromagnetically coupled(*16*)(*17*).

There are also other types of copper proteins. They can be summarized as follows: (a) Multi-Copper Oxidases: These enzymes contain Type I, II and III centers in various stoichiometric ratios such as L-ascorbate oxidase, laccase and ceruloplasmin(*11*)(*18*). Ascorbate oxidase and laccase catalyze the reduction of oxygen to water. But ceruloplasmin is an ancient multicopper oxidase that has ferroxidase activity and functions as an antioxidant(*18*). (b) Copper centers in cytochrome c-oxidase and nitrous oxide reductase: the copper centers appear to be

unique in these cases. In addition to a Type II copper site, these proteins contain a Cu_A center that consists of two copper ions connected by two bridging cysteine thiolates. The Cu_A site has very distinct EPR and UV/Vis spectra[19][20]. There is evidence that the copper ions form a mixed valence copper pair having 1.5+ charge per Cu[21]. A recent addition to the copper protein typology is the "Type zero" protein by Gray *et al*. They built a novel Cu(II) binding site by incorporating new amino acid residues at Cys112 position in *Pseudomonas aeruginosa* azurin. This mutant does not resemble any of the existing types mentioned above. X-ray crystallographic analysis has shown that this copper site adopts a distorted tetrahedral geometry with an unusually short Cu–O bond with the carbonyl of Gly45. Type zero proteins also have a relatively weak absorption near 800 nm and a narrow parallel hyperfine splitting in their EPR spectra[22].

1.2.1 *Azurin: Central protein of this research*

Azurin is found in several gram-negative bacteria e.g. *Pseudomonas aeruginosa, P. aureofaciens, P. chlorophis, P. fluorescens, P. putida, Alcaligenes denitrificans, A. xylosoxidans, A. faecalis, Bordetella bronchiseptica* and *Streptomyces thioluteus* (*23*).The present studies have been performed on azurin from *Pseudomonas aeruginosa.* The azurin gene encodes a signal peptide-containing protein consistent with a periplasmic location of the mature protein. Azurin is excreted to the periplasmic space, where the signal peptide is cleaved off during translocation by a signal peptidase. There is strong evidence that the protein fulfills a role in the oxidative stress-induced response in its parent host organism[24]. Recently, azurin from the bacteria *Pseudomonas aeruginosa* has been reported to induce and trigger apoptosis in human cancer cells[25][26]. One of the recent biosensing-applications for azurin is the detection of superoxide species *in vitro*(*27*)(*24*)(*28*)(*29*).

Azurin is a small soluble Type I blue copper protein with molecular weight of 13,998 kDa. A large number of three-dimensional structures have been solved by X-ray crystallography or NMR(*23*)(*30*)(*31*). The copper ligands are His46, Cys112, and His117. Two weaker axial ligands are provided by Met121 and the carbonyl oxygen of Gly45 (Fig. 1.2). The active site shows a slightly distorted trigonal bipyramidal geometry in which the copper ion is only 0.1 Å out of the N_2S plane (*32*). In the so-called "northern region" of the protein, the copper ion is buried at 0.7 nm distance from the surface. Azurin is composed of 128 amino acids with eight β-

strands forming two β-sheets in a Greek-key motif. These are connected by a α-helix. This produces considerable rigidity of the polypeptide matrix. [33][34][35]. On the opposite side of Cu-center, in the so-called southern corner of the protein, close to the N-terminus, the presence of a disulfide bond between Cys3 and Cys26 contributes to the stability of the protein. Upon removal of the copper, the protein is significantly destabilized[36][37][38]. It has a typical UV/Vis absorption around 595-630 nm originating from a π-π* transition in the molecular orbital scheme of the oxidized copper site[39][40] (Fig. 1.2). This transition mainly involves the $d_{x^2-y^2}$-orbital on the copper and the 3p-orbital of the Cys112-sulfur [41][42]. Upon reduction, the strong blue color disappears due to the d^{10} electronic configuration of copper. This change in absorption spectrum allows us to monitor the oxidation state of the protein by optical techniques[43][44]. There is only one single tryptophan residue at position 48 in azurin which is buried inside the hydrophobic core of the protein. The absorption and fluorescence maxima of the tryptophan occur at 291 nm and 309 nm, respectively (Fig. 1.3). One of the Cu ligands, His117, protrudes through the surface of the protein, and it connects the copper ion with the surroundings of the protein. The so-called hydrophobic patch around His117 consists of a number of apolar amino acid residues which facilitate the formation of electron-transfer (ET) complexes[45]. The redox properties of azurin are dictated by the copper site. The redox potential of Cu-azurin depends on pH, and amounts to 310 mV (vs. NHE) at pH 7.0[46][47][48]. The copper ion in azurin can also be reconstituted with Zn^{2+}. The resulting zinc-azurin is redox inactive and is often used for control experiments.
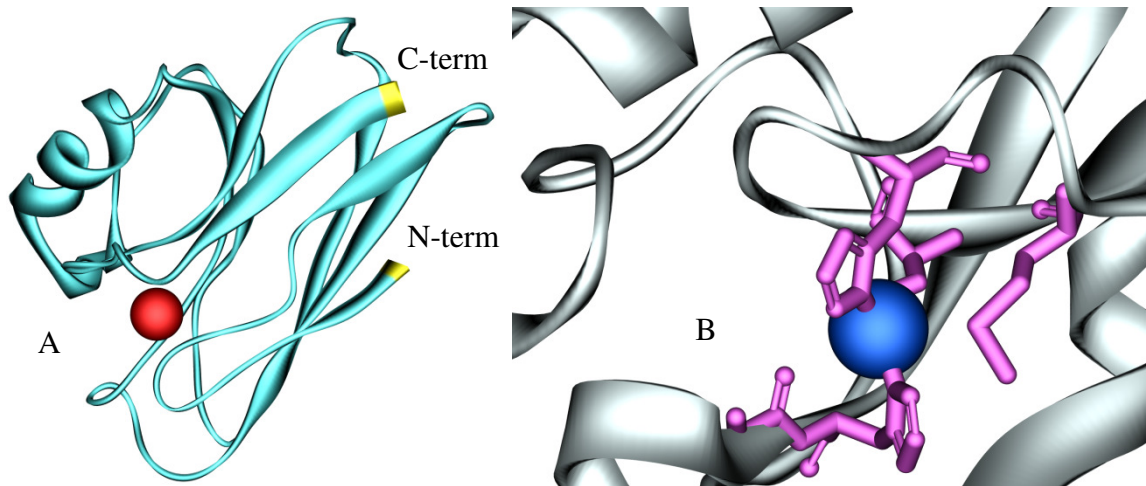
Figure 1.2: *Ribbon presentation of azurin from Pseudomonas aeruginosa. The copper ion is shown as a red sphere. C-terminus and the N-terminus have been marked in yellow. (B) Close-up of the active site. Copper is shown as a blue sphere. The pink ball and sticks display the active site ligands of the copper (His117, His46, Cys112, Met121, and Gly45).*
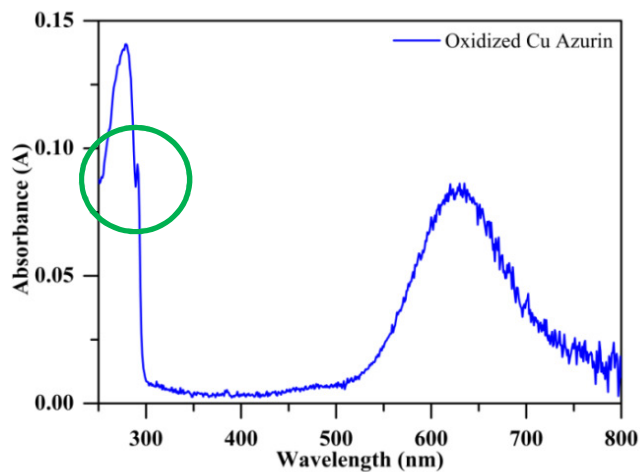
Figure 1.3: *UV-vis spectrum of 14 µM azurin from P. aeruginosa in 20 mM HEPES, pH 7.0 in the oxidized form. The shoulder at 291 nm is marked by a green circle and is due to the presence of single tryptophan residue in azurin.*

1.3 *Fluorophores*

The key fluorophores used in fluorescence based biochemical assays are categorized into three groups(*49*)(*50*)(*51*)(*52*)(*53*)(*54*) (See Fig. 1.4 for example). The first group corresponds to the natural fluorophores such as flavins, the indole ring of tryptophan, tyrosines, nicotinamide

adenine dinucleotide (NADH) and chlorophyll(*50*). The second group comprises fluorescent molecules whose optical properties are sensitive to the presence of a particular molecule or ion e.g. Na^+, Ca^{2+}, Mg^{2+}, Cl^-(*50*). Finally, in cases, where the molecule of interest is non-fluorescent, or its intrinsic fluorescence is too low or in the wrong wavelength region, one can label or fuse it with an external probe. This external probe can be either an intrinsically fluorescent protein such as a green fluorescent protein (GFP), a chimeric fused protein or a small organic compound(*50*). A recent addition to the collection of fluorescent labels refers to nanometer sized quantum dots(*55*). Their emission depends on the size of the particle but all quantum dots can be excited with near UV light.

In the present thesis, we used small organic fluorophores (extrinsic) to label azurin(*56*)(*57*)(*58*)(*59*)(*60*). These extrinsic chromophores were attached covalently for example by a maleimide for sulfhydryl labeling, or a succinimidyl ester for the labeling of primary amines(*54*)(*56*)(*58*). The labeling reactions can be controlled by the pH of the solution. Lysine-derived amines and the N-terminus of the protein are the primary targets for the labeling reactions by succinimidyl esters. They are good nucleophiles, and lysines are more reactive than the N-terminus above pH 8.0 (*pKa* = 9.18)(*58*). (*61*)(*62*)(*63*). Thiols are reactive at neutral pH allowing the selective coupling to fluorophores even in the presence of amines.
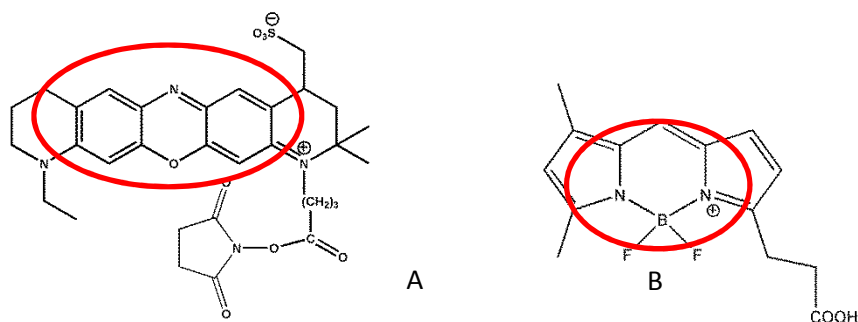
Figure 1.4: *Chemical structures of two commonly used fluorophores: (A) ATTO655 NHS (group 1) and (B) BODIPY FL carboxy (group 2). The red circled regions display the chromophoric zones of the dyes.*

1.4 *Fluorescence and Förster Resonance Energy Transfer (FRET)*

The origin of fluorescence phenomenon can be illustrated with a simple three electronic-state diagram as proposed by Alexander Jablonski (See Fig. 1.5)(*50*). The diagram shows the ground state (S_0), the first excited singlet state (S_1), 2nd excited singlet state (S_2) and triplet state (T_1) respectively. Each of them carries a series of vibrational states. Molecules are excited by an

external source, e.g. an incandescent lamp or a laser, and they relax back to the ground state (S_0) thereby emitting fluorescence (red arrow) on a timescale of nanoseconds. The orange dotted line represents the fast internal conversion from S_2 to S_1. The molecules in the S_1 state can also undergo a transition to T_1, which is called inter-system crossing (blue arrow). As the transition-probability from T_1 to S_0 is low, long-lived phosphorescence (dotted red arrow) often occurs on a millisecond to second time scale. Fluorescence resonance energy transfer (FRET) is an energy transfer between two molecules by which a donor molecule transfers its excitation energy to an acceptor molecule without emission of a photon(*64*)(*49*)(*65*)(*66*). Förster, Stryer, and Haugland described how the FRET efficiency, *E*, depends on the donor-acceptor separation between two atoms or molecules(*49*). According to Eqn. 1.1

$$E = R_0{}^6/(R_0{}^6 + r^6) \qquad\qquad (1.1)$$
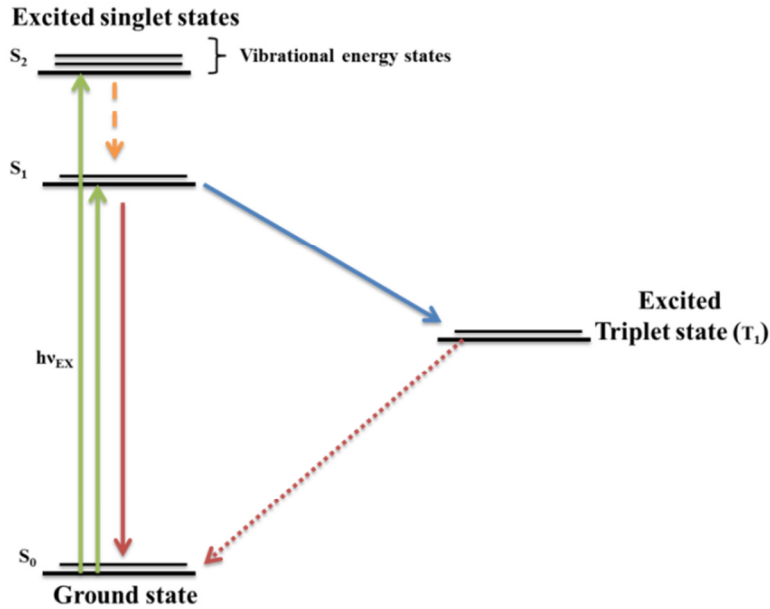
Figure 1.5: *A Jablonski diagram depicting the electronic states involved in the processes of excitation and emission. S_0 represents the electronic ground state of the molecule; S_1 and S_2 are the 1st and 2nd excited singlet states. Each state contains vibrational levels, a few of which are indicated in the diagram. T_1 is the lowest triplet state. Green arrows: excitation; red arrow: emission; blue arrow: S_1 to T_1 transition.*

where *r* represents the distance between the donor and the acceptor, and R_0 is the Förster radius. R_0 is the distance at which the energy transfer efficiency is 50%. The Förster radius depends on the spectral features of the donor and acceptor as follows:

$$R_0 = 0.211[\kappa^2\eta^{-4}Q_DJ(\lambda)]^{1/6} \qquad (1.2)$$

where κ is the dipole orientation factor, η is the refractive index of the medium, Q_D is the quantum yield of the donor, and $J(\lambda)$ is the overlap integral defined as

$$J(\lambda) = \int_0^\infty I_D(\lambda)\varepsilon_A(\lambda)\lambda^4 d\lambda \Big/ \int_0^\infty I_D(\lambda)d\lambda \qquad (1.3)$$

where $I_D(\lambda)$ is termed the fluorescence intensity of the donor and $\varepsilon_A(\lambda)$ is the extinction coefficient of the acceptor molecule at the wavelength λ. The energy transfer efficiency, E, is given by

$$E = 1 - (\tau^f_{DA}/\tau^f_D) = 1 - (F_{DA}/F_D) \qquad (1.4)$$

where $\tau^f_{D \text{ and}} \tau^f_{DA}$ are fluorescence lifetimes of the donor in the absence and in the presence of the acceptor, respectively, and F_D and F_{DA} stand for the fluorescence intensities of the donor in the absence and the presence of the acceptor, respectively.

FRET-based applications can be found in the fields of biosensor design, single molecule imaging of cells, molecular motors, DNA mechanical movements, etc.

1.4.1 *The FluRedox principle: FRET as a reporter of the redox state of the proteins*

The FRET-based FluRedox technique monitors the redox state of a metalloprotein via fluorescence detection (Fig. 1.6). The emission of a covalently attached fluorophore (donor) reflects the changes in the absorbance of the prosthetic group (FRET acceptor). Cu-azurin, exploited in the current thesis, in its oxidized form shows an absorbance maximum at 628 nm which overlaps with the fluorescence emission of ATTO655 dye (Fig. 1.7). The energy transfer, i.e. the FRET, is high in this form, and the fluorescence of the dye is quenched. However, FRET is low when the copper azurin is reduced since the 628 nm absorption disappears upon the reduction of the proteins. Successful applications of this principle have been reported(*6*)(*44*)(*67*)(*68*)(*69*).

No FRET, High fluorescence **FRET, low fluorescence intensity**

Oxidation

Reduction

Cu^{1+} Cu^{2+}
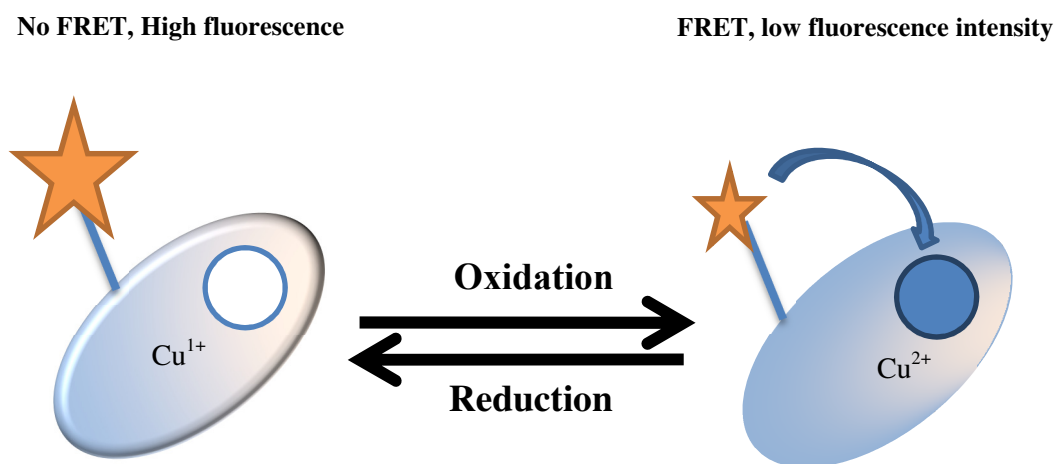
Figure 1.6: *Illustration of the FluRedox principle. On the left-hand side, the fluorescence of the label is high, and no FRET occurs due to the reduction of the cofactor in the active site of the protein; at the right side, the fluorescence of the label is quenched due to FRET between the label and the cofactor of the protein and fluorescence is low. The label is shown as an orange star.*
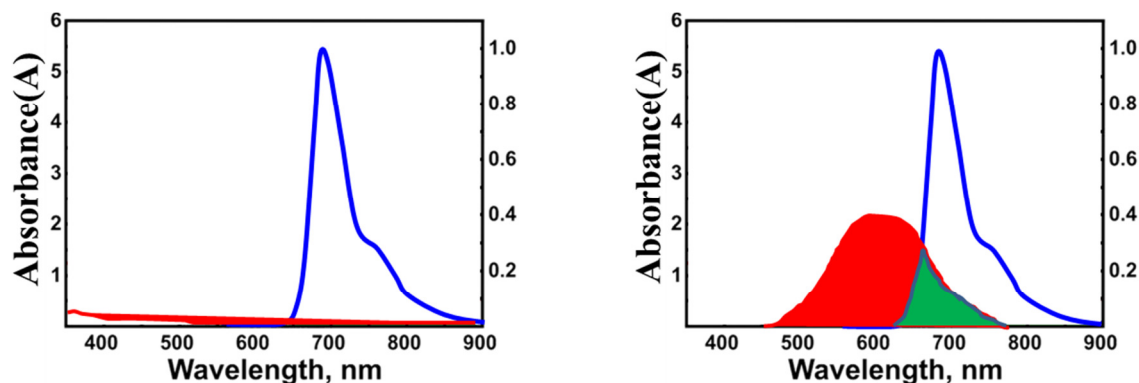
Figure 1.7: *Example of spectral overlap between the absorption spectra of a cupredoxin and the emission of a dye. In the left panel, the red line displays the absorption spectrum of the reduced form of the protein and the right panel shows the spectrum of the oxidized form. The green area is the overlap with the emission spectrum (blue line) of the dye.*

1.5 *Single-Molecule Techniques*

Single-molecule fluorescence techniques such as Fluorescence correlation spectroscopy (FCS), Fluorescence lifetime imaging (FLIM), Photobleaching FRET, Light Sheet Microscopy provide new and detailed information about (*70*)(*8*)(*9*)(*10*)(*71*)(*72*)(*73*)(*74*)(*75*)(*76*) enzyme mechanisms, protein-protein interactions, conformational changes of a molecule, molecular reaction dynamics, etc., at single molecule level. For exhaustive reviews of these achievements see(*76*)(*77*)(*78*). Here an introduction to the methodologies used in the present thesis is presented.

1.5.1 *Fluorescence Correlation Spectroscopy*

In a simple fluorescence correlation spectroscopy (FCS) setup (Fig. 1.8) the fluorescent sample is kept on a stage, and a laser of a particular wavelength is focused in the sample through an objective lens with high numerical aperture (Fig.1.9). The emitted light passes through the same objective and a pinhole of micrometer size and is subsequently detected with a photo diode. The small pinhole helps to eliminate out-of-focus fluorescence from the image plane of the objective. Thus, a high signal to noise ratio is obtained from a fluorescent sample. The optical setup (Fig. 1.8) produces a tiny observation or detection volume which is in the order of femtoliters and the fluorescent signals from diffusing molecules can be collected and analyzed. If the number of molecules in the detection volume is small, we can observe single molecular events from the labeled molecules in the form of signal fluctuations (*79*)(*80*)(*81*)(*82*)(*83*)(*84*).

The observation time of the fluorescently labeled molecule is limited by the residence time of that molecule inside the detection volume.

FCS makes use of the autocorrelation function $G(\tau)$. First, the signal from the sample is recorded as a fluorescence trace, $F(t)$. The autocorrelation function is then defined as

$$G(\tau) = <\delta F(t) \times \delta F(t+\tau)>/<F(t)>^2 \qquad (1.6)$$

where brackets "$< >$" denote averaging over time t, $\delta F(t)=F(t)-<F(t)>$ and τ is a variable interval. This function therefore, computes its self-similarity after a lag time τ. It contains information about equilibrium concentrations, reaction kinetics and diffusion rates of molecules in the sample of interest. For example, if a labeled molecule moves in and out of the detection volume, the autocorrelation curve may look as depicted in Fig. 1.10.
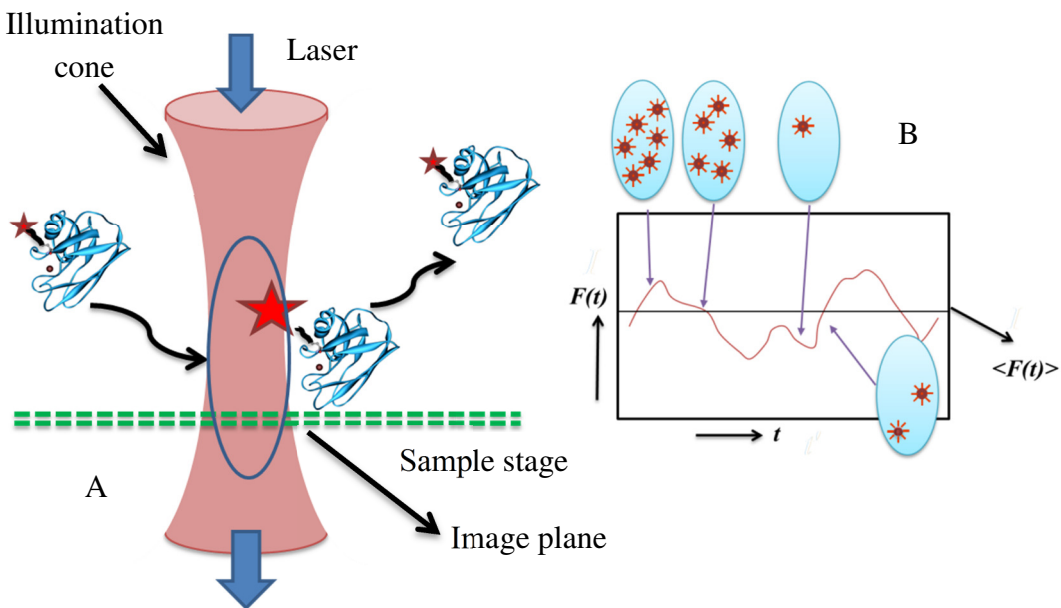
Figure 1.8: *(A) Zoomed view of the detection volume (blue ellipsoid): the red illumination cone represents the laser beam and a labeled protein moves in and out of the focus; (B) the recorded fluorescence intensity signal (red line) fluctuates.*
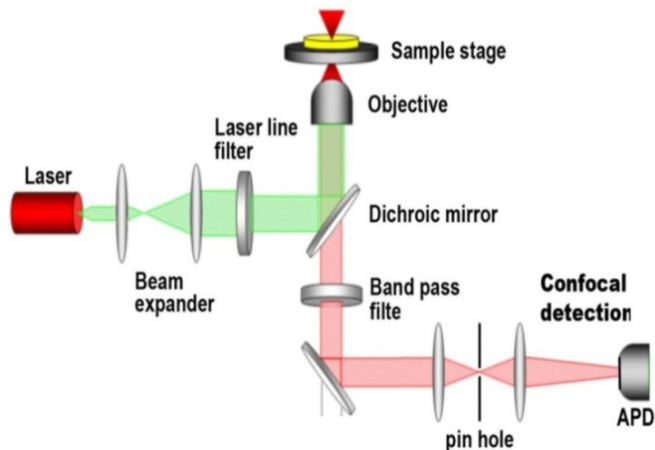
Figure 1.9: *A simplified diagram of the FCS setup. The instrumentation for FCS will be discussed in Chapter 2. The fluorescent sample is kept on a sample stage (gray) and a laser beam (green) of a particular wavelength is focused in the sample through filters, a dichroic mirror and an objective lens. Then, the emitted light or fluorescence (red) is passed through the same objective, dichroic mirror, and a micron size pinhole. The fluorescence is detected at an avalanche photodiode (APD) (gray).*
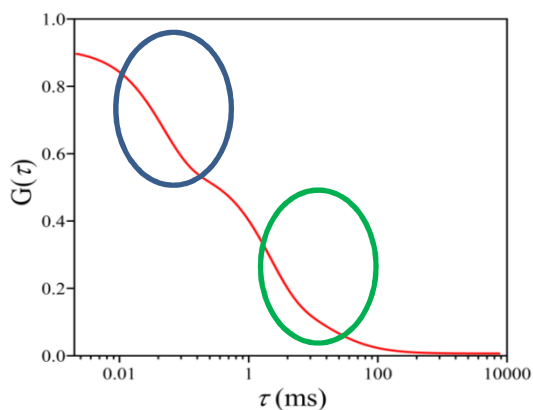
Figure 1.10: *Example of an autocorrelation curve (red). The green circled region corresponds with the diffusion of the particle, the blue circled region corresponds with a reaction that is faster than diffusion.*

The calculation of the autocorrelation function is based on the assumption that the light intensity in the detection volume has approximately a three-dimensional Gaussian profile. This results in(85)

$$G(\tau) = G(0) \cdot \left(1 + \frac{4D\tau}{r_0^2}\right)^{-1} \cdot \left(1 + \frac{4D\tau}{z_0^2}\right)^{-\frac{1}{2}}$$

$$= G(0) \cdot \left(1 + \frac{\tau}{\tau_D}\right)^{-1} \cdot \left(1 + \left(\frac{r_0}{z_0}\right)^2 \frac{\tau}{\tau_D}\right)^{-\frac{1}{2}}$$

$$= G(0) \cdot \left(1 + \frac{\tau}{\tau_D}\right)^{-1} \cdot \left(1 + \frac{\tau}{k^2 \tau_D}\right)^{-\frac{1}{2}} \qquad (1.7)$$

where $\qquad \tau_D = \dfrac{r_0^2}{4D}$,

and $\qquad k = \dfrac{z_0}{r_0}$.

D is the diffusion coefficient of the molecule of interest, τ_D is the residence time of the molecule in the detection volume and r_0 and z_0 denote the distances from the center of the observation volume to the point where the intensity has dropped by a factor of $1/e^2$ in the radial and axial direction, respectively.

$G(0)$ is given by

$$G(0) = \frac{1}{\langle N \rangle} = \frac{1}{c \cdot V_{eff} \cdot N_A} \qquad (1.8)$$

where, $<N>$ corresponds to the average number of particles in the detection volume, c is the sample concentration of the molecule of interest, V_{eff} is the effective detection volume, and N_A is Avogadro's constant. V_{eff} is larger by a factor of $2^{(2/3)}$ than the confocal volume, which is calculated on the basis of a Gaussian intensity profile.

Compared to classical measurements, FCS is a special technique in the sense that the molecular dynamics on different time scales can be investigated in a single measurement. Photochemical reactions can induce changes in fluorescence intensity. As the time window in

FCS ranges typically from 10^{-12} sec to several seconds(*86*)(*87*)(*88*), those changes can be observed in the autocorrelation curve as depicted in the example of Fig. 1.10. The decay at the short time scale corresponds with a reaction that modifies the fluorescence of the molecule like triplet state blinking, FRET-induced quenching, protonation or electron transfer. From such a decay the reaction rate and the steady-state population of the molecules with the reaction can be investigated. When more than one reaction occurs, the expression for the autocorrelation functions becomes:

$$G(\tau)=G(0)G_{diff}(\tau)G_1(\tau)...G_n(\tau) \qquad (1.9)$$

with
$$G_i(\tau) = \frac{1 - F_i + F_i e^{-\frac{\tau}{\tau_i}}}{1 - F_i} \qquad (i=1,2...n)$$

where $F_1,...F_n$ are the fractions of fluorescent molecules associated with having relaxation times $\tau_1, ...\tau_n$ respectively. In Chapters 3 and 4, equations 1.7-1.9 will be used to analyze inter- and intra-molecular ET reactions in ATTO655 labeled azurin.

1.6 *Electron transfer (ET) theory*

Redox proteins are nanoscale electronic devices. They can convert energy from one form to another(*89*)(*90*)(*91*) by driving electrons and protons. Copper proteins containing blue sites mostly function as electron carriers and are involved in biological energy conversions and biochemical transformations. Possessing two oxidation states and a wide range of redox potentials (200-1000 mV) are functional advantages of these proteins to mediate electrons(*92*)(*93*). Our understanding of the electronic and functional properties of copper proteins has dramatically advanced partly due to the availability of high-resolution crystal structures and model complexes. In the following paragraph, a short review of ET theory and expressions for the rates of electron transfer between a weakly coupled donor and an acceptor are given.

The investigation of ET kinetics was started over 50 years ago. (*94*)(*95*). Because electrons move much faster than nuclei, the nuclei remain fixed during ET reactions (Franck-

Condon Principle). The transition state for such a reaction must lie at a point in the nuclear-configuration space where the reactant and product states are degenerate. This means that the only instant at which an electron can shuttle between two species occurs when both have achieved the same nuclear configuration as a result of thermally induced fluctuations. Thus, the kinetics of the reaction depends on an activation barrier ($\Delta G^\dagger$) (Fig. 1.11). In general, the factors that control the rate constant of electron transfer (k_{ET}) include the distance (r) between donor and acceptor, the Gibbs free energy of activation, and the reorganization energy of the reaction. The rate of the electron-transfer process is given by(*96*)

$$k_{ET} = \frac{2\pi}{h} \frac{H^2_{DA}}{\sqrt{4\pi\lambda k_B T}} e^{-\frac{(\Delta G^0_{CS} + \lambda)^2}{4\lambda k_B T}} \qquad (1.10)$$
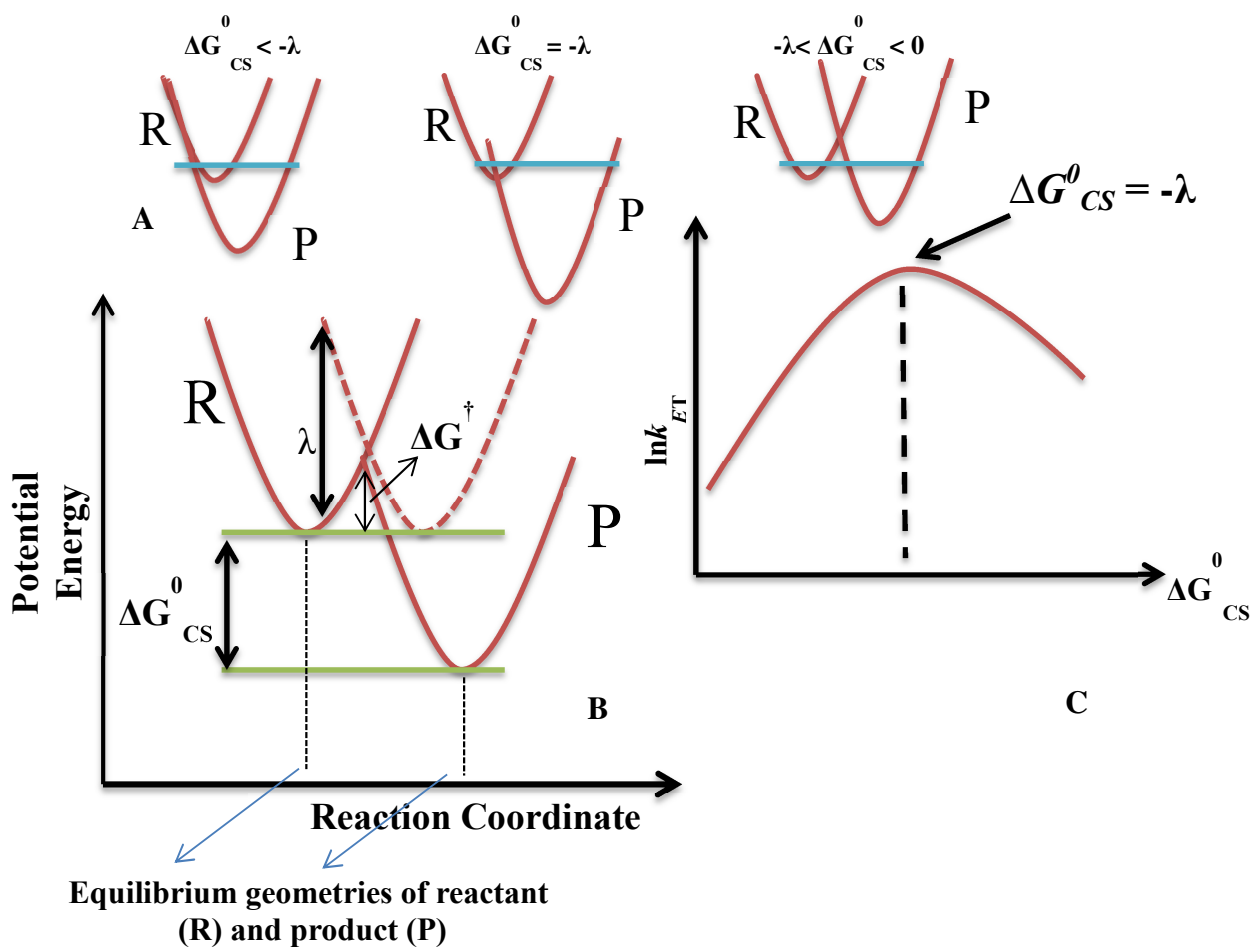
Figure 1.11: *A schematic potential energy diagram for electron transfer. Reactant and Product are represented by R and P. Their nuclear motions are sketched as single harmonic oscillators. The activation energy of the reaction depends on the free energy of the reaction and the reorganization energy [Adapted from Quarterly Reviews of Biophysics 2003, 36(3), pp. 341–372]*

- H_{DA} determines the electronic coupling between donor and acceptor and is generally represented as

$$H_{DA}^2 = H_0^2 \, exp[-\beta(r-r_0)] \qquad (1.11)$$

where r_0 is the distance when donor and acceptor are in direct contact, β is the distance-decay constant presenting the efficiency of the ET reaction in the protein medium. It can vary between 1.4Å^{-1} to 0.7Å^{-1} depending on the secondary structure of the protein *(96)(97)(98)(99)(100)(101)(102)*.

- The activation energy, $\Delta G^{\dagger}$, is related to the standard reaction Gibbs free energy (ΔG_{CS}^{0}) and the reorganization energy (λ), and is given by (*96*)(*103*)(*104*)

$$\Delta G^{\dagger} = \frac{(\Delta G^{0}{}_{CS} + \lambda)^{2}}{4\lambda} \qquad (1.12)$$

This $\Delta G^{0}{}_{CS}$ is the free-energy change for the charge-separation and can be estimated using the Rehm-Weller approach to be described in Chapter 2.

- The ET between donor and acceptor often results in molecular rearrangement of the reactants. The energy required for this rearrangement before ET is called the reorganization energy (λ). It is a combination of changes in the nuclear configuartion of the redox centers (changes in bond angles and lengths) and the surrounding solvent and protein matrix during ET. For a high ET rate, the reorganization energy has to be small. k_{B} is the Boltzmann constant, and T is the temperature expressed in Kelvin.

A profile for the potential energy curve has been displayed schematically in Fig. 1.11. Reactant (R) is converted into the product (P) after ET. A plot of $\ln k_{ET}$ vs. ΔG^{0} has (Fig. 1.11 C) a bell-shape.(*96*)(*105*)(*104*). The following regimes are usually distinguished.

- a normal regime for small driving forces ($-\lambda < \Delta G^{0} < 0$) in which the process is thermally activated and $\ln k_{ET}$ increases with increasing driving force;
- an activationless regime in which a change in driving force does not cause large changes in the reaction rate, and where $-\lambda = \Delta G^{0}$.
- an "inverted" regime for strongly exergonic processes ($-\lambda > \Delta G^{0}$) in which $\ln k_{ET}$ decreases with increasing driving force.

The plot illustrates that the ET rate will increase with $-\Delta G^{0}$ until a maximum rate is observed for $-\Delta G^{0} = \lambda$ and the rate then decreases.

In essence, Marcus semi-classical theory suggests that an electron can travel from one redox center to another one over a limited distance. ET may occur through space or by hopping, or the electron can travel through covalent and hydrogen bonds to reach its destination [(*96*) and references therein]. The effect of parameters like distance, redox potential, and temperature on ET rates has been well established theoretically as well as experimentally(*106*)(*107*)(*108*).

1.7 *Scope of this thesis*

Chapter 2 reports the calibration of the instrumental setup required for the FCS measurements. Calibration was performed by using a commercially available organic dye, ATTO655, and recording its fluorescence intensity over time at different concentrations. The instrumental factor "*k*" obtained from the calibration measurements, has been used for the fitting of the autocorrelation curves of labeled Zn and Cu azurin samples in Chapter 3, 4 and 5. Chapter 2 also includes a general discussion of bimolecular interactions and photoinduced electron transfer reactions in proteins.

In **Chapter 3**, the species obtained from labeling of zinc azurin with ATTO655 are analyzed by using FCS. The analysis of the autocorrelation functions report on the bimolecular ET reactions between the dye and the redox chemicals [ascorbate, potassium hexacyanoferrate (II) or (III)].

Chapter 4 reports on the photoinduced electron transfer reactions in labeled copper azurin. First, the species obtained from labeling copper azurin with ATTO655 are analyzed by using FCS. The analysis of the autocorrelation functions reports on the microsecond dynamics of the intramolecular ET reactions between the dye and redox-active center. It is shown that in oxidoreductases photoinduced intra-molecular electron-transfer (PET) between the label and active center may occur over long distances and is not restricted to situations where the label is in Van-der-Waals contact with the redox center.

Chapter 5 describes an extensive study of Cu-Azurin variants (K122Q and K122S). We use FCS to study the ET kinetics between the dye and the copper center in copper azurin variants. Our first strategy was to label the variants with ATTO655 and characterize the products of the labeling reactions between the label ATTO655 and the blue copper azurin and then extend our investigation into the properties of a specific labeled species under redox conditions using FCS. The analysis reveals that intramolecular photoinduced electron transfer (PET) can reach the sub-millisecond time scale depending on the position of the Cu-label on the azurin surface. Finally, the distance dependences of the FRET and PET rates on the Cu-label distance are compared.

At the end, a general conclusion is presented, and the perspectives are discussed.

References

(1) Holm, R. H.; Kennepohl, P.; Solomon, E. I. Structural and Functional Aspects of Metal Sites in Biology. *Chem. Rev.* **1996**, *96*, 2239–2314.

(2) Thomson, A. J.; Gray, H. B. Bio-inorganic chemistry. *Curr. Opin. Chem. Biol.* **1998**, *2*, 155–158.

(3) Gilardi, G.; Fantuzzi, a; Sadeghi, S. J. Engineering and design in the bioelectrochemistry of metalloproteins. *Curr. Opin. Struct. Biol.* **2001**, *11*, 491–9.

(4) Zhang, J.; Chi, Q.; Hansen, A. G.; Jensen, P. S.; Salvatore, P.; Ulstrup, J. Interfacial electrochemical electron transfer in biology - towards the level of the single molecule. *FEBS Lett.* **2012**, *586*, 526–35.

(5) Schuler, B.; Eaton, W. A. Protein folding studied by single-molecule FRET. *Curr. Opin. Struct. Biol.* **2008**, *18*, 16–26.

(6) Kuznetsova, S.; Zauner, G.; Aartsma, T. J.; Engelkamp, H.; Hatzakis, N.; Rowan, A. E.; Nolte, R. J. M.; Christianen, P. C. M.; Canters, G. W. The enzyme mechanism of nitrite reductase studied at single-molecule level. *Proc. Natl. Acad. Sci. U. S. A.* **2008**, *105*, 3250–3255.

(7) Elmalk, A. T.; Salverda, J. M.; Tabares, L. C.; Canters, G. W.; Aartsma, T. J. Probing redox proteins on a gold surface by single molecule fluorescence spectroscopy. *J. Chem. Phys.* **2012**, *136*, 235101.

(8) Chen, P.; Andoy, N. M. Single-molecule fluorescence studies from a bioinorganic perspective. *Inorganica Chim. Acta* **2008**, *361*, 809–819.

(9) Wang, Q.; Goldsmith, R. H.; Jiang, Y.; Bockenhauer, S. D.; Moerner, W. E. Probing single biomolecules in solution using the anti-Brownian electrokinetic (ABEL) trap. *Acc. Chem. Res.* **2012**, *45*, 1955–64.

(10) Mollova, E. T. Single-molecule fluorescence of nucleic acids. *Curr. Opin. Chem. Biol.* **2002**, *6*, 823–828.

(11) Solomon, E. I.; Sundaram, U. M.; Machonkin, T. E. Multicopper Oxidases and Oxygenases. *Chem. Rev.* **1996**, *96*, 2563–2606.

(12) Solomon, E. I. Electronic structures of active sites in copper proteins: Contributions to reactivity. *J. Inorg. Biochem.* **1993**, *51*, 450.

(13) Holwerda, R. a; Wherland, S.; Gray, H. B. Electron transfer reactions of copper proteins. *Annu. Rev. Biophys. Bioeng.* **1976**, *5*, 363–396.

(14) Pérez-Henarejos SA, Alcaraz LA, D. A. Blue Copper Proteins: A rigid machine for efficient electron transfer, a flexible device for metal uptake. *Arch. Biochem. Bophysics* **2015**, *584*, 134–148.

(15) Klinman, J. P. Mechanisms whereby mononuclear copper proteins functionalize organic substrates. *Chem. Rev.* **1996**, *96*, 2541–2562.

(16) Lewis, E. a.; Tolman, W. B. Reactivity of Dioxygen-Copper Systems. *Chem. Rev.* **2004**,

104, 1047–1076.

(17) Filion, L. 3.2 A structure of the copper containing oxygen carrying protein Panulirus interruptus haemocyanine. *Nature* **1984**, *309*, 23–29.

(18) Hellman, N. E.; Gitlin, J. D. Ceruloplasmin metabolism and function. *Annu. Rev. Nutr.* **2002**, *22*, 439–458.

(19) Paumann, M.; Lubura, B.; Regelsberger, G.; Feichtinger, M.; Köllensberger, G.; Jakopitsch, C.; Furtmüller, P. G.; Peschek, G. A.; Obinger, C. Soluble CuA Domain of Cyanobacterial Cytochrome c Oxidase. *J. Biol. Chem.* **2004**, *279*, 10293–10303.

(20) Lappalainen, P.; Aasa, R.; Malmström, B. G.; Saraste, M. Soluble CuA-binding domain from the Paracoccus cytochrome c oxidase. *J. Biol. Chem.* **1993**, *268*, 26416–26421.

(21) Fee, J. a; Choc, M. G.; Findling, K. L.; Lorence, R.; Yoshida, T. Properties of a copper-containing cytochrome c1aa3 complex: a terminal oxidase of the extreme thermophile Thermus thermophilus HB8. *Proc. Natl. Acad. Sci. U. S. A.* **1980**, *77*, 147–151.

(22) Lancaster, K. M.; Debeer, S.; Yokoyama, K.; Richards, J. H.; Gray, H. B. Type Zero Copper proteins. *NIH Public Access* **2010**, *1*, 711–715.

(23) Kolczak, U., Dennison, C., Messerschmidt, A., and Canters, G. W. *Handbook of Metalloproteins*; Messerschmidt, A., Huber, R., Poulos, T. L., and Wieghardt, K., Ed.; John Wiley & Sons, Ltd: Chichester, 2001.

(24) Yang, D. S.; Miao, X. D.; Ye, Z. M.; Feng, J.; Xu, R. Z.; Huang, X.; Ge, F. F. Bacterial redox protein azurin induce apoptosis in human osteosarcoma U2OS cells. *Pharmacol. Res.* **2005**, *52*, 413–421.

(25) Yamada, T.; Goto, M.; Punj, V.; Zaborina, O.; Chen, M. L.; Kimbara, K.; Majumdar, D.; Cunningham, E.; Das Gupta, T. K.; Chakrabarty, A. M. Bacterial redox protein azurin, tumor suppressor protein p53, and regression of cancer. *Proc. Natl. Acad. Sci. U. S. A.* **2002**, *99*, 14098–103.

(26) Ananda M Chakrabartya Bacterial azurin in potential cancer therapy. *Cell Cycle* **2016**.

(27) Yamada, T.; Goto, M.; Punj, V.; Zaborina, O.; Kimbara, K.; Das Gupta, T. K.; Chakrabarty, a. M. The bacterial redox protein azurin induces apoptosis in J774 macrophages through complex formation and stabilization of the tumor suppressor protein p53. *Infect. Immun.* **2002**, *70*, 7054–7062.

(28) Yamada, T.; Hiraoka, Y.; Ikehata, M.; Kimbara, K.; Avner, B. S.; Das Gupta, T. K.; Chakrabarty, A. M. Apoptosis or growth arrest: Modulation of tumor suppressor p53's specificity by bacterial redox protein azurin. *Proc. Natl. Acad. Sci. U. S. A.* **2004**, *101*, 4770–4775.

(29) Shleev, S.; Wetterö, J.; Magnusson, K. E.; Ruzgas, T. Electrochemical characterization and application of azurin-modified gold electrodes for detection of superoxide. *Biosens. Bioelectron.* **2006**, *22*, 213–219.

(30) Adman, E. T. and Jensen, L. H. Structural Features of Azurin at 2.7 Å Resolution. *Isr. J. Chem.* **1981**, *21*, 8–12.

(31)   Nar, H.; Messerschmidt, a.; Van De Kamp, M.; Canters, G. W.; Huber, R. Crystal structure analysis of oxidized Pseudomonas aeruginosa azurin at pH 5.5 and pH 9.0. A pH-induced conformational transition involves a peptide bond flip. *J. Mol. Biol.* **1991**, *221*, 765–772.

(32)   Nar, H.; Messerschmidt, A.; Huber, R.; Van De Kamp, M.; Canters, G. W. Crystal structure analysis of oxidized Pseudomonas aeruginosa azurin at pH 5.5 and pH 9.0. A pH-induced conformational transition involves a peptide bond flip. *J. Mol. Biol.* **1991**, *221*, 765–772.

(33)   Engeseth, H. R.; McMillin, D. R. Studies of thermally induced denaturation of azurin and azurin derivatives by differential scanning calorimetry: evidence for copper selectivity. *Biochemistry* **1986**, *25*, 2448–2455.

(34)   Leckner, J.; Bonander, N.; Wittung-Stafshede, P.; Malmström, B. G.; Karlsson, B. G. The effect of the metal ion on the folding energetics of azurin: A comparison of the native, zinc and apoprotein. *Biochim. Biophys. Acta - Protein Struct. Mol. Enzymol.* **1997**, *1342*, 19–27.

(35)   Carmelo Rosa, Danilo Milardi, Domenico Grasso, Rita Guzzi, L. S. Thermodynamics of the thermal unfolding of azurin. *J. Phys. Chem.* **1995**, *99*, 14864–14870.

(36)   Palm-Espling, M. E.; Niemiec, M. S.; Wittung-Stafshede, P. Role of metal in folding and stability of copper proteins in vitro. *Biochim. Biophys. Acta - Mol. Cell Res.* **2012**, *1823*, 1594–1603.

(37)   Leckner, J. Folding and structure of azurin - The influence of a metal. *Thesis-Chalmers Univ. Technol.* **2001**.

(38)   Pozdnyakova, I.; Guidry, J.; Wittung-Stafshede, P. Studies of Pseudomonas aeruginosa azurin mutants: cavities in beta-barrel do not affect refolding speed. *Biophys. J.* **2002**, *82*, 2645–2651.

(39)   Dennison, C. Investigating the structure and function of cupredoxins. *Coord. Chem. Rev.* **2005**, *249*, 3025–3054.

(40)   Gray, H. B.; Malmström, B. G.; Williams, R. J. Copper coordination in blue proteins. *J. Biol. Inorg. Chem. JBIC a Publ. Soc. Biol. Inorg. Chem.* **2000**, *5*, 551–559.

(41)   Lowery, M.; Solomon, E. Axial ligand bonding in blue copper proteins. *Inorganica Chim. Acta* **1992**, *200*, 233–243.

(42)   Solomon, E.; Hare, J. Spectroscopic studies of stellacyanin, plastocyanin, and azurin. Electronic structure of the blue copper sites. *J. Am. Chem. Soc.* **1980**, *102*, 168–178.

(43)   Schmauder, R.; Alagaratnam, S.; Chan, C.; Schmidt, T.; Canters, G. W.; Aartsma, T. J. Sensitive detection of the redox state of copper proteins using fluorescence. *J. Biol. Inorg. Chem.* **2005**, *10*, 683–687.

(44)   Kuznetsova, S.; Zauner, G.; Schmauder, R.; Mayboroda, O. A.; Deelder, A. M.; Aartsma, T. J.; Canters, G. W. A Förster-resonance-energy transfer-based method for fluorescence detection of the protein redox state. *Anal. Biochem.* **2006**, *350*, 52–60.

(45) Kamp, M. Van De; Floris, R. Site-directed mutagenesis reveals that the hydrophobic patch of azurin mediates electron transfer. *J. Am. Chem. Soc.* **1990**, *112*, 907–908.

(46) Van de Kamp M1, Canters GW, Andrew CR, Sanders-Loehr J, Bender CJ, P. J. Effect of lysine ionization on the structure and electrochemical behaviour of the Met44-->Lys mutant of the blue-copper protein azurin from Pseudomonas aeruginosa. *Eur. J. Biochem.* **1993**, *218*, 229–238.

(47) van de Kamp, M.; Canters, G. W.; Wijmenga, S. S.; Lommen, A.; Hilbers, C. W.; Nar, H.; Messerschmidt, A.; Huber, R. Complete sequential 1H and 15N nuclear magnetic resonance assignments and solution secondary structure of the blue copper protein azurin from Pseudomonas aeruginosa. *Biochemistry* **1992**, *31*, 10194–10207.

(48) Farver, O.; Skov, L. K.; Van De Kamp, M.; Canters, G. W.; Pecht, I. The effect of driving force on intramolecular electron transfer in proteins. Studies on single-site mutated azurins. *Eur. J. Biochem.* **1992**, *210*, 399–403.

(49) Stryer, L.; Haugland, R. P. Energy transfer: a spectroscopic ruler. *Proc. Natl. Acad. Sci. U. S. A.* **1967**, *58*, 719–726.

(50) Lakowicz, J. R. *Principles of Fluorescence Spectroscopy*; 2006.

(51) Shimomura,O., Saiga, Y., and Johnson, F. H. Fluorescence Energy transfer. *Fed. Proc.* **1962**, 401–03.

(52) Zauner, G.; Lonardi, E.; Bubacco, L.; Aartsma, T. J.; Canters, G. W.; Tepper, A. W. J. W. Tryptophan-to-dye fluorescence energy transfer applied to oxygen sensing by using type-3 copper proteins. *Chem. - A Eur. J.* **2007**, *13*, 7085–7090.

(53) Chalfie, M.; Tu, Y.; Euskirchen, G.; Ward, W. W.; Prasher, D. C. Green fluorescent protein as a marker for gene expression. *Science* **1994**, *263*, 802–805.

(54) Ernst, L. a; Gupta, R. K.; Mujumdar, R. B.; Waggoner, a S. Cyanine dye labeling reagents for sulfhydryl groups. *Cytometry* **1989**, *10*, 3–10.

(55) Ruan, G.; Winter, J. O. Alternating-color quantum dot nanocomposites for particle tracking. *Nano Lett.* **2011**, *11*, 941–945.

(56) Panchuk-Voloshina, N.; Haugland, R. P.; Bishop-Stewart, J.; Bhalgat, M. K.; Millard, P. J.; Mao, F.; Leung, W. Y.; Haugland, R. P. Alexa dyes, a series of new fluorescent dyes that yield exceptionally bright, photostable conjugates. *J. Histochem. Cytochem.* **1999**, *47*, 1179–1188.

(57) Sauer, M.; Han, K. T.; Müller, R.; Nord, S.; Schulz, a.; Seeger, S.; Wolfrum, J.; Arden-Jacob, J.; Deltau, G.; Marx, N. J.; Zander, C.; Drexhage, K. H. New fluorescent dyes in the red region for biodiagnostics. *J. Fluoresc.* **1995**, *5*, 247–261.

(58) Brinkley, M. A brief survey of methods for preparing protein conjugates with dyes, haptens, and cross-linking reagents. *Bioconjug. Chem.* **1992**, *3*, 2–13.

(59) Mujumdar, R. B.; Ernst, L. a; Mujumdar, S. R.; Lewis, C. J.; Waggoner, a S. Cyanine dye labeling reagents: sulfoindocyanine succinimidyl esters. *Bioconjug. Chem.* **1993**, *4*, 105–111.

(60) Buschmann, V.; Weston, K. D.; Sauer, M. Spectroscopic study and evaluation of red-absorbing fluorescent dyes. *Bioconjug. Chem.* **2003**, *14*, 195–204.

(61) Lina F. Bernal-Perez, Laszlo Prokai, Y. R. Selective N-terminal fluorescent labeling of proteins using 4-chloro-7-nitrobenzofurazan: A method to distinguish protein N-terminal acetylation. *Anal. Biochem.* **2012**, *428*, 13–15.

(62) Chan, A. O.-Y.; Ho, C.; Chong, H.; Leung, Y.-C.; Huang, J.; Wong, M.; Che, C. Modification of N-terminal α-amino groups of peptides and proteins using ketenes. *J. Am. Chem. Soc.* **2012**, *134*, 2589–98.

(63) Williamson, D. J.; Fascione, M. A.; Webb, M. E.; Turnbull, W. B. Efficient N-Terminal Labeling of Proteins by Use of Sortase. *Angew. Chemie Int. Ed.* **2012**, *51*, 9377–9380.

(64) Förster, T.; Energiewanderung, Z.; Von, F. Zwischenmolekulare Energiewanderung und Fluoreszenz. *Ann. Phys.* **1939**, *248*, 55–75.

(65) Clegg, R. M. Fluorescence resonance energy transfer. *Curr. Opin. Biotechnol.* **1995**, *6*, 103–110.

(66) Steinberg, I. Z. Long-range nonradiative transfer of electronic excitation energy in proteins and polypeptides. *Annu. Rev. Biochem.* **1971**, *40*, 83–114.

(67) Schmauder, R.; Alagaratnam, S.; Chan, C.; Schmidt, T.; Canters, G. W.; Aartsma, T. J. Sensitive detection of the redox state of copper proteins using fluorescence. *J. Biol. Inorg. Chem.* **2005**, *10*, 683–7.

(68) Schmauder, R.; Librizzi, F.; Canters, G. W.; Schmidt, T.; Aartsma, T. J. The oxidation state of a protein observed molecule-by-molecule. *Chemphyschem* **2005**, *6*, 1381–6.

(69) Gustiananda, M.; Andreoni, A.; Tabares, L. C.; Tepper, A. W. J. W.; Fortunato, L.; Aartsma, T. J.; Canters, G. W. Sensitive detection of histamine using fluorescently labeled oxido-reductases. *Biosens. Bioelectron.* **2012**, *31*, 419–25.

(70) Edman, L.; Mets, U.; Rigler, R. Conformational transitions monitored for single molecules in solution. *Proc. Natl. Acad. Sci. U. S. A.* **1996**, *93*, 6710–6715.

(71) Xie, X. S. Single-Molecule Approach to Enzymology. *Single Mol.* **2001**, *2*, 229–236.

(72) Eggeling, C.; Widengren, J.; Brand, L.; Schaffer, J.; Felekyan, S.; Seidel, C. A. M. Analysis of photobleaching in single-molecule multicolor excitation and Förster resonance energy transfer measurements. *J. Phys. Chem. A* **2006**, *110*, 2979–95.

(73) Dittrich, P.; Schwille, P. Photobleaching and stabilization of fluorophores used for single-molecule analysis with one- and two-photon excitation. *Appl. Phys. BLasers Opt.* **2001**, *73*, 829–837.

(74) Lu, H. P.; Xie, X. S. Single-Molecule Kinetics of Interfacial Electron Transfer. **1997**, *5647*, 2753–2757.

(75) Cordes, T.; Maiser, A.; Steinhauer, C.; Schermelleh, L.; Tinnefeld, P. Mechanisms and advancement of antifading agents for fluorescence microscopy and single-molecule spectroscopy. *Phys. Chem. Chem. Phys.* **2011**, *13*, 6699–709.

(76)   Bustamante, C. In singulo biochemistry: when less is more. *Annu. Rev. Biochem.* **2008**, *77*, 45–50.

(77)   Piehler, J. New methodologies for measuring protein interactions in vivo and in vitro. *Curr. Opin. Struct. Biol.* **2005**, *15*, 4–14.

(78)   Ha, T.; Selvin, P. R. The New Era of Biology In Singulo. *Cold Spring Harb. Lab. Press* **2008**, 1–36.

(79)   Ries, J.; Schwille, P. Fluorescence correlation spectroscopy. *BioEssays* **2012**, *34*, 361–368.

(80)   Elson, E. L. Fluorescence correlation spectroscopy: Past, present, future. *Biophys. J.* **2011**, *101*, 2855–2870.

(81)   Bacia, K.; Kim, S. A.; Schwille, P. Fluorescence cross-correlation spectroscopy in living cells. *Nat. Methods* **2006**, *3*, 83–89.

(82)   Hess, S. T.; Huang, S.; Heikal, A. A.; Webb, W. W. Biological and chemical applications of fluorescence correlation spectroscopy: A review. *Biochemistry* **2002**, *41*, 697–705.

(83)   Chiantia, S.; Ries, J.; Schwille, P. Fluorescence correlation spectroscopy in membrane structure elucidation. *Biochim. Biophys. Acta* **2009**, *1788*, 225–233.

(84)   Widengren, J.; Rigler, R.; Mets, Ü. Triplet-state monitoring by fluorescence correlation spectroscopy. *J. Fluoresc.* **1994**, *4*, 255–258.

(85)   Ries, J.; Schwille, P. Fluorescence correlation spectroscopy. *Bioessays* **2012**, *34*, 361–8.

(86)   Kapusta, P.; Wahl, M.; Benda, A.; Hof, M.; Enderlein, J. FLCS - Fluorescence lifetime correlation spectroscopy. *SymPhoTime* **2007**, *17*, 43–8.

(87)   Rüttinger, S.; Kapusta, P.; Patting, M.; Wahl, M.; Macdonald, R. On the resolution capabilities and limits of fluorescence lifetime correlation spectroscopy (FLCS) measurements. *J. Fluoresc.* **2010**, *20*, 105–14.

(88)   Kapusta, P.; Wahl, M.; Benda, A.; Hof, M.; Enderlein, J. Fluorescence lifetime correlation spectroscopy. *J. Fluoresc.* **2007**, *17*, 43–8.

(89)   Artés, J. M.; López-Martínez, M.; Díez-Pérez, I.; Sanz, F.; Gorostiza, P. Nanoscale charge transfer in redox proteins and DNA: Towards biomolecular electronics. *Electrochim. Acta* **2014**, *140*, 83–95.

(90)   Aviram, A.; Ratner, M. A. Molecular rectifiers. *Chem. Phys. Lett.* **1974**, *29*, 277–283.

(91)   Kuznetsov, a. M.; Ulstrup, J. Theory of electron transfer at electrified interfaces. *Electrochim. Acta* **2000**, *45*, 2339–2361.

(92)   Farver, O.; Pecht, I. Electron transfer in blue copper proteins. *Coord. Chem. Rev.* **2011**, *255*, 757–773.

(93)   Canters, G. W.; Gilardi, G. Engineering type 1 copper sites in proteins. *FEBS Lett* **1993**, *325*, 39–48.

(94)   Marcus, R. A.; Sutin, N. Electron transfers in chemistry and biology. *Biochim. Biophys.*

Acta - Rev. Bioenerg. **1985**, *811*, 265–322.

(95) Marcus, R. A. Electron Transfer Reactions in Chemistry: Theory and Experiment. *Angew. Chemie Int. Ed.* **1993**, *32*, 1111–1121.

(96) Winkler, J. R.; Gray, H. B. Long-range electron tunneling. *J. Am. Chem. Soc.* **2014**, *136*, 2930–2939.

(97) C. C. Moser, C. C. Page, X. Chen, P. L. D. Biological electron tunneling through native protein media. *J. Biol. Inorg. Chem.* **1997**, *2*, 393–398.

(98) Winkler, J. R.; Gray, H. B. Electron tunneling in proteins: Role of the intervening medium. *J. Biol. Inorg. Chem.* **1997**, *2*, 399–404.

(99) Beratan, D. N.; Betts, J. N.; Onuchic, J. N. Protein electron transfer rates set by the bridging secondary and tertiary structure. *Science (80-.).* **1991**, *252*, 1285–1288.

(100) Beratan, D. N.; Onuchic, J. N.; Winkler, J. R.; Gray, H. B. Electron-tunneling pathways in proteins. *Science* **1992**, *258*, 1740–1741.

(101) Page, C. C.; Moser, C. C.; Chen, X.; Dutton, P. L. Natural engineering principles of electron tunnelling in biological oxidation-reduction. *Nature* **1999**, *402*, 47–52.

(102) Moser, C. C.; Keske, J. M.; Warncke, K.; Farid, R. S.; Dutton, P. L. Nature of biological electron transfer. *Nature* **1992**, *355*, 796–802.

(103) Gray, H. B.; Winkler, J. R. Long-range electron transfer. *Proc. Natl. Acad. Sci. U. S. A.* **2005**, *102*, 3534–3539.

(104) Paola Ceroni and Vincenzo Balzani Photoinduced Energy and Electron Transfer Processes. In *The Exploration of Supramolecular Systems and Nanostructures by Photochemical Techniques*; 2012; pp. 21–38.

(105) Gray, H. B.; Winkler, J. R. Long-range electron transfer. *Proc. Natl. Acad. Sci. U. S. A.* **2005**, *102*, 3534–9.

(106) Gray, H. B.; Winkler, J. R. Electron flow through metalloproteins. *Biochim. Biophys. Acta* **2010**, *1797*, 1563–72.

(107) Chi, Q.; Zhang, J.; Jensen, P. S.; Christensen, H. E. M.; Ulstrup, J. Long-range interfacial electron transfer of metalloproteins based on molecular wiring assemblies. *Faraday Discuss.* **2006**, *131*, 181–195; discussion 205–220.

(108) McLendon, G.; Hake, R. Interprotein electron transfer. *Chem. Rev.* **1992**, *92*, 481–490.